IEEE Access
Multidisciplinary ⋮ Rapid Review ⋮ Open Access Journal

Received 27 March 2024, accepted 18 April 2024, date of publication 25 April 2024, date of current version 3 May 2024.

Digital Object Identifier 10.1109/ACCESS.2024.3393837

RESEARCH ARTICLE

Adaptive Feedforward Cancellation for Precise Repetitive Motion in Coarse-Fine Control System

SHOTA YABUI[1], (Member, IEEE), HARUKI MURAKAMI[1], (Member, IEEE), TAKENORI ATSUMI[2], (Member, IEEE), AND YUSUKE UCHIYAMA[3]

[1]Faculty of Science and Engineering, Mechanical Systems Engineering, Tokyo City University, Setagaya-ku, Tokyo 158-8557, Japan
[2]Chiba Institute of Technology, Narashino, Chiba 275-0016, Japan
[3]MAZIN Inc., Chuo-ku, Tokyo 103-0023, Japan

Corresponding author: Shota Yabui (yabuis@tcu.ac.jp)

This work was supported by the Research Grant from the Mazda Foundation.

ABSTRACT This paper introduces a novel control scheme to achieve precise repetitive motion within a dual-input-single-output (DISO) system consisting of course-actuator and fine-actuator. Repetitive motion stands as a crucial operation in various applications, particularly in manufacturing processes. Designing a control system capable of accurately tracking reference signals during repetitive motion is imperative for DISO systems. The proposed method focuses on adaptive feed-forward cancellation (AFC) to effectively compensate for position error signals related to the reference signal. A typical control scheme implements AFC for the entire control loop. In the control system, the same characteristic of AFC works for both actuators in the DISO control system. The same AFC output is working to both actuators. On the other hand, the proposed control scheme implements AFC to each actuator. It can generate suitable AFC output for the course-actuator, fine-actuator, respectively. That is, the major contribution of proposed control scheme individually optimizes the AFC in the course-fine control system. This design approach significantly enhances the control performance of DISO systems, considering the distinctive characteristics and stroke limitations of the actuators. Experimental implementation of the proposed control system validated its efficacy, affirming the improvement of control performance in DISO systems.

INDEX TERMS Dual-input-single-output (DISO) system, repetitive control, adaptive feedforward cancellation, loop shaping.

I. INTRODUCTION

Control design methodologies play a pivotal role in achieving desirable dynamics in mechatronic systems [1]. In the pursuit of enhanced control performance, certain mechatronic systems incorporate dual actuator systems, including piezo-electric dual-stage tape [2], head positioning control systems for hard disk drives [3], servo systems for optical mechatronic applications [4], and wafer stage control systems in manufacturing [5]. These systems are characterized as dual-input-single-output (DISO) systems.

One of the common functionalities in these mechanical systems involves repetitive motion, found in patterned movements, manufacturing processes, and various applications [6], [7]. In such scenarios, precise tracking of a reference signal during repetitive motion is crucial. Given that the reference signal exhibits periodic frequency components, minimizing periodic error signals becomes imperative for enhancing tracking performance.

This study centers on adaptive feed-forward cancellation (AFC) to mitigate periodic error signals [8], [9]. Developed to compensate for position error signals induced by periodic disturbances, AFC's efficacy has been validated in previous mechatronic system studies. To optimize its effectiveness, a critical consideration involves the apt design of parameters within the adaptive algorithm. Various sophisticated design methods for AFC implementation in single-input-single-output (SISO) systems exist, rooted in classical control

The associate editor coordinating the review of this manuscript and approving it for publication was Zhiguang Feng.

theory, modern control theory, and the like [10]. Contrastingly, addressing narrow-band disturbances, particularly periodic disturbances in DISO systems, often relies on the Youla-Kucera (YK) parametrization [11], iterative learning control (ILC) [12], and the AFC [13]. This design method allows the transformation of DISO system structures into SISO system block diagrams. In this transformed SISO system, servo engineers can apply established SISO controller design methods, facilitating the design of a unified controller for both actuators [14], [15]. This approach proves effective in compensating for position error signals, offering manageability in DISO system control design. While servo engineers can evaluate the overall control system performance, designing controllers that account for the unique characteristics of each actuator remains a challenge. The introduction of dual-actuator systems aims to enhance control performance through coarse-fine motion control, utilizing actuators with distinct characteristics. Consequently, the control system can be tailored to accommodate different controllers for each actuator.

In this paper, we propose an AFC design method tailored for achieving precise repetitive motion in DISO systems. The previous control scheme implements the AFC to entire control loop [11], [12], [13]. The parameters of AFC are designed to the open loop characteristics summing up the that of course actuator and fine actuator. In the control system, the same characteristic of AFC works for both actuators in the DISO control system. The same AFC output is working to both actuators. On the other hand, the proposed control scheme implements AFC to each actuator, namely course actuator and fine actuator. The parameters of AFC are designed to each open loop. In the proposed control system, the AFC is individually optimized for each actuator which has different characteristic (frequency response). The suitable AFC output works for each actuator, respectively. As a result, the proposed control scheme can control the DISO system finely with comparison to the previous control scheme. The proposed control scheme employing AFC and design method for individually optimization method for each actuator are presented in this paper.

The proposed method emphasizes three key aspects to enhance positioning performance during repetitive motion. First, it asserts that AFC effectively reduces position error signals in repetitive motion. As the reference signal of repetitive motion consists of specific frequency components, AFC works to compensate for the position error signal caused by these frequency components. Second, the method considers the stroke limitations of each actuator in the DISO system. Each actuator in the DISO system has a different stroke for coarse-fine motion control, with the coarse actuator having a large stroke and the fine actuator having a small stroke. The proposed design method avoids performance degradation due to system uncertainty and operates each actuator within its stroke limitation. Third, the entire control system with AFC demonstrates robustness against uncertainties in system variations. Mass production

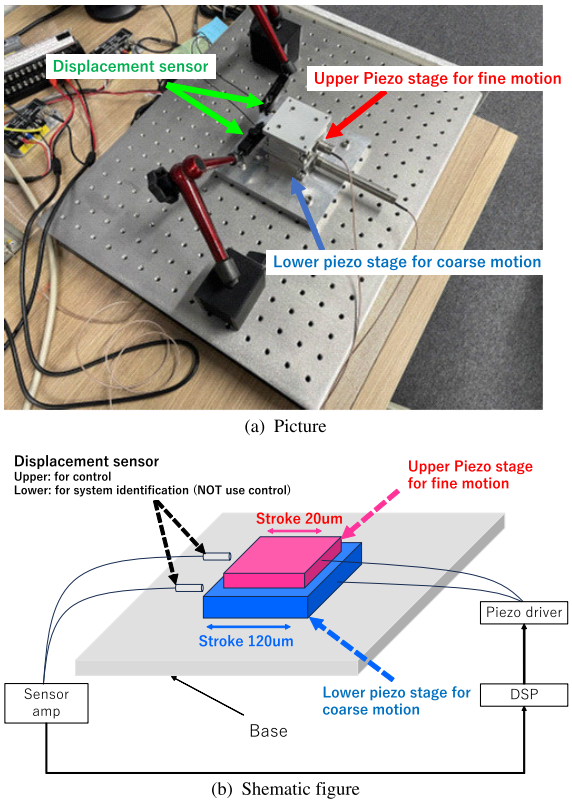

FIGURE 1. Experimental system of the DISO system.

systems, such as disk drives, exhibit individual variation, and wafer stage systems must maintain consistent performance across diverse operating conditions. The effectiveness of this approach was verified in the experimental system.

II. EXPERIMENTAL SYSTEM

This section introduces the experimental setup, depicted in both a picture and a schematic figure, as illustrated in Fig. 1. For the development of the DISO system, distinct types of piezo actuators are employed: the lower piezo actuator MF-120 and the upper piezo actuator MF-20, both manufactured by MESS-TEK Co., Ltd. The displacement sensors used are PU-03 from AEC, measuring the stage displacement on the upper piezo actuator. The system operates with voltage as the input signal to the piezo actuator and measures the resulting displacement using sensors. The lower piezo actuator serves as the coarse actuator with a larger stroke of 120μm for coarse adjustments, while the upper piezo actuator functions as the fine actuator with a smaller stroke of 20μm for fine adjustments. The control objective is the positioning of the displacement of the upper piezo actuator, and both actuators move in the same direction, as depicted in Fig. 1(b). he displacement of the lower piezo actuator and the upper piezo actuator is denoted as y_{lp} and y_{up}, respectively. The total displacement y_{p0} is calculated as $y_{p0} = y_{lp} + y_{up}$. The displacement is generated by the input signal of the lower piezo actuator, u_{lp}, and that of the upper piezo actuator, u_{up}. Note that, the displacement signal y_{lp} is used for system identification, and this characteristic is not

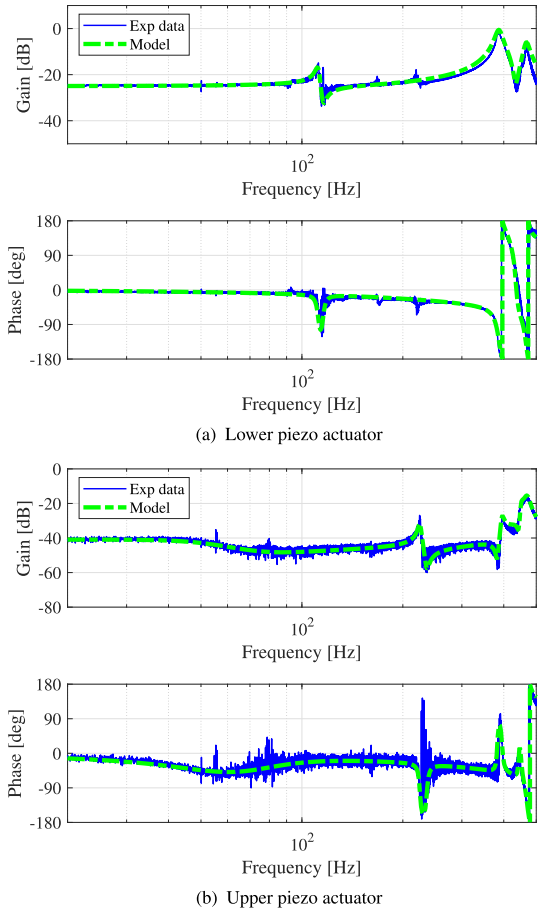

FIGURE 2. Frequency responses of control objective.

leveraged directly for the positioning control. A digital signal processor (DSP) generates the voltage signal based on the measured total displacement signal, y_p.

In this study, the main design strategy for the control system is the loop shaping method. Consequently, the performance of the control system is designed based on the frequency transfer function and evaluated through the frequency response. These responses are derived from the amplitude spectrum of input and output data obtained via a sine sweep test. The frequency responses of the lower and upper piezo actuators are illustrated in Fig. 2. Resonant modes are evident in both actuators, with differences in frequency responses under 300 Hz. Especially, the frequency and gain of the lowest resonant frequency in each actuator exhibit distinct forms. The transfer function of the lower piezo actuator, P_{lp}, is defined as the following function.

$$P_{lp}(s) = \sum_{i=1}^{4} \frac{\alpha_{lpi}}{s^2 + 2\zeta_{lpi}\omega_{lpi}s + \omega_{lpi}^2} \tag{1}$$

The transfer function of the upper piezo actuator, P_{up}, is defined as following function.

$$P_{up}(s) = \sum_{i=1}^{5} \frac{\alpha_{upi}}{s^2 + 2\zeta_{upi}\omega_{upi}s + \omega_{upi}^2} \tag{2}$$

TABLE 1. Parameters of $P_{lp}(s)$.

i	ω_{lpi}	α_{lpi}	ζ_{lpi}
1	$112 \times 2\pi$	1500	0.015
2	$387 \times 2\pi$	240000	0.025
3	$425 \times 2\pi$	-100000	0.05
4	$467 \times 2\pi$	150000	0.02

TABLE 2. Parameters of $P_{up}(s)$.

i	ω_{upi}	α_{upi}	ζ_{upi}
1	$55 \times 2\pi$	50	0.5
2	$225 \times 2\pi$	1000	0.01
3	$395 \times 2\pi$	-5000	0.01
4	$450 \times 2\pi$	-15000	0.01
5	$470 \times 2\pi$	60000	0.02

The parameters, α_{lpi}, ζ_{lpi}, ω_{lpi}, α_{upi}, ζ_{upi}, and ω_{upi}, are listed in Table 1 and Table 2. These parameters are obtained through curve fitting for the frequency responses of the lower piezo actuator and upper piezo actuator. The frequency response of $P_{lp}(s)$, $P_{up}(s)$ is plotted in Fig. 2 as a dashed line. These frequency responses are matched to the measurement data. Fig. 4 illustrates the time responses of direct motion ranging from u_{lp} to y_{lp} and from u_{up} to y_{up}, along with those of coupling motion, ranging from u_{lp} to y_{up} and from u_{up} to y_{lp}. The amplitude of coupling motion is significantly smaller than that of direct motion. Therefore, the coupling motion can be ignored in this experimental system.

III. BASIC CONTROL SYSTEM OF DISO

This section presents the proposed design method aimed at achieving precise repetitive motion in the DISO system. The fundamental block diagram of this system is illustrated in Fig. 4. Herein, r is the reference signal, e is the position error signal, C_{lp} is the feedback controller of the lower piezo actuator, C_{up} is the feedback controller of the upper piezo actuator, and K is the displacement sensor. As the controller is implemented in the DSP, C_{lp} and C_{up} are discrete-time controllers. The sampling time of K is $T_s = 0.0005$, k is the sample number, and t is time. We design the controllers, C_{lp} and C_{up}, with enough margin for the stability criteria. $P_{lp}(z)$ and $P_{up}(z)$ are the discretized transfer function of $P_{lp}(s)$, $P_{up}(s)$. $C_{lp}(z)$ and $C_{up}(z)$ are defined as following function.

$$C_{lp}(z) = C_{mlp}(z)N_{lp} \tag{3}$$

$$C_{mlp}(z) = \frac{1.86 - 1.14\,z^{-1} - 1.86\,z^{-2} + 1.14\,z^{-3}}{1 - 2.52\,z^{-1} + 2.04\,z^{-2} - 0.52\,z^{-3}} \tag{4}$$

$$C_{up}(z) = C_{mup}(z)N_{up} \tag{5}$$

$$C_{mup}(z) = \frac{74.85 - 59.07\,z^{-1} - 74.85\,z^{-2} + 59.07\,z^{-3}}{1 - 2.10\,z^{-1} + 1.45\,z^{-2} - 0.33\,z^{-3}} \tag{6}$$

Herein, C_{mlp} and C_{mup} are the main feedback controllers of the lower and upper piezo actuators, respectively. The one-step delay operator is denoted z^{-1}.

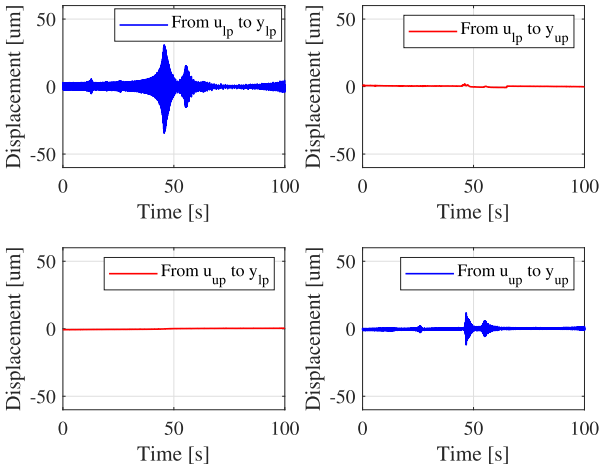

FIGURE 3. Time responses of direct motion and coupling motion.

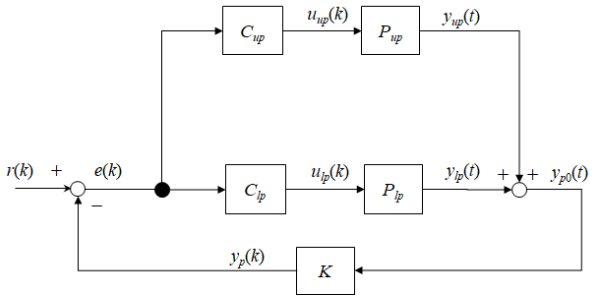

FIGURE 4. The basic block diagram of the DISO control system.

N_{lp} and N_{up} are notch filters of the lower and upper piezo actuators, respectively. In this study, the basic control system is designed to have sufficient stability performance for validation of the AFC, and it is designed not to excite the mechanical resonance of the piezo stage. Specifically, the maximum gain of sensitivity function is targeted to be less than 3dB in the frequency range of 100 - 500Hz. In addition, the sensitivity function gain is to be 0dB at the frequency where mechanical resonance exists. For ease of understanding, the notch filter is represented by continuous-time transfer functions as following equations.

$$N_{lps}(s) = \sum_{i=1}^{4} \frac{s^2 + 2\zeta_{lpni}\omega_{lpni}s + \omega_{lpni}^2}{s^2 + 2\zeta_{lpdi}\omega_{lpdi}s + \omega_{lpdi}^2} \tag{7}$$

$$N_{ups}(s) = \sum_{i=1}^{4} \frac{s^2 + 2\zeta_{upni}\omega_{upni}s + \omega_{upni}^2}{s^2 + 2\zeta_{updi}\omega_{updi}s + \omega_{updi}^2} \tag{8}$$

When implementing, use the transfer functions are discretized by the matched z-transformation as following equations.

$$N_{lp}(z) = \sum_{i=1}^{4} \frac{n_{lpai} + n_{lpbi}z^{-1} + n_{lpci}z^{-2}}{1 + n_{lpdi}z^{-1} + n_{lpei}z^{-2}} \tag{9}$$

$$N_{up}(z) = \sum_{i=1}^{4} \frac{n_{upai} + n_{upbi}z^{-1} + n_{upci}z^{-2}}{1 + n_{updi}z^{-1} + n_{upei}z^{-2}} \tag{10}$$

TABLE 3. Parameter of notch filters for lower piezo actuator.

(a) Parameters of N_{lps}

Roll	i	ζ_{lpni}	ζ_{lpdi}	ω_{lpni}	ω_{lpdi}
Mechanical resonance compensation	1	0.02	0.40	$112\times2\pi$	$112\times2\pi$
	2	0.02	0.50	$387\times2\pi$	$387\times2\pi$
	3	0.02	0.50	$467\times2\pi$	$467\times2\pi$
Loop shaping	4	0.01	0.50	$230\times2\pi$	$230\times2\pi$

(b) Parameters of N_{lp} (discretized of N_{lps})

Roll	i	n_{lpai}	n_{lpbi}	n_{lpci}	n_{lpdi}	n_{lpei}
Mechanical resonance compensation	1	0.878	- 1.64	0.866	- 1.65	0.755
	2	0.595	- 0.404	0.566	- 0.539	0.297
	3	0.544	- 0.110	0.513	- 0.284	0.231
Loop shaping	4	0.718	- 1.07	0.707	- 1.13	0.486

TABLE 4. Parameter of notch filters for upper piezo actuator.

(a) Parameters of N_{ups}

Roll	i	ζ_{upni}	ζ_{updi}	ω_{upni}	ω_{updi}
Mechanical resonance compensation	1	0.005	0.50	$225\times2\pi$	$225\times2\pi$
	2	0.03	0.50	$395\times2\pi$	$395\times2\pi$
	3	0.02	0.50	$470\times2\pi$	$470\times2\pi$
Loop shaping	4	0.10	0.50	$160\times2\pi$	$160\times2\pi$

(b) Parameters of N_{up} (discretized of N_{ups})

Roll	i	n_{upai}	n_{upbi}	n_{upci}	n_{updi}	n_{upei}
Mechanical resonance compensation	1	0.719	- 1.09	0.715	- 1.15	0.493
	2	0.600	- 0.373	0.554	- 0.512	0.289
	3	0.542	- 0.099	0.511	- 0.275	0.228
Loop shaping	4	0.826	- 1.38	0.747	- 1.41	0.605

The design procedure of four notch filters for each actuator is as following.

- Lower piezo actuator: N_{lps}, N_{lp}
  Three notch filters are designed to compensate for the mechanical resonances at 112Hz, 387Hz, and 467Hz as shown in Fig. 2(a). The center frequencies ω_{lpni} and ω_{lpdi} are set to match these frequencies. The parameters ζ_{lpni} and ζ_{lpdi} are set to achieve a sensitivity function gain of 0dB with reference to the width and depth of these mechanical resonances [16]. Furthermore, one notch filter is designed for loop shaping, and the parameters are set the sensitivity function gain around 230Hz less than 3dB.
- Upper piezo actuator: N_{ups}, N_{up}
  Three notch filters are designed to compensate for the mechanical resonances at 225Hz, 395Hz, and 470Hz as shown in Fig. 2(b). The center frequencies ω_{upni} and ω_{updi} are set to match these frequencies. The parameters ζ_{upni} and ζ_{updi} are set to achieve a sensitivity function gain of 0dB with reference to the width and depth of these mechanical resonances [16]. Furthermore, one notch filter is designed for loop shaping, and the parameters are set the sensitivity function gain around 160Hz less than 3dB.

The parameters of N_{lps}, N_{ups}, N_{lp} and N_{up} are listed in Table 3(a), Table 3(b), Table 4(a), and Table 4(b).

The design results of the control system are depicted in Fig. 5, wherein, L_{lp}, L_{up}, and L_{tp} denote the lower, upper, and total actuator loops, respectively. S_{tp} denotes the sensitivity

of the total actuator loop.

$$L_{lp}(z) = P_{dlp}(z)C_{lp}(z), L_{up}(z) = P_{dup}(z)C_{up}(z),$$
$$L_{tp}(z) = L_{lp}(z) + L_{up}(z),$$
$$S_{tp}(z) = \frac{1}{1 + L_{tp}(z)}$$

where P_{dlp} and P_{dup} are the discretized transfer functions of P_{lp} and P_{up}, respectively. The design results of the control system are illustrated in Fig. 5. The gain margin and phase margin of the control system are satisfactory: 17.39 dB and 79.87 deg, respectively. Particularly, the maximum gain of S_{tp} is less than 3 dB, indicating a sufficient stability margin [17].

IV. PRECISE REPETITIVE MOTION IN DISO SYSTEM IMPLEMENTATION OF AFC

This section demonstrates the implementation of Adaptive Feedforward Control (AFC) for achieving precise repetitive motion in the DISO system. To showcase repetitive motion, a 10 Hz square wave signal is set as r in the control system, where the objective is to follow the signal, namely $r = y_p$. The time responses of r, y_p, and e are depicted in Fig. 6. The shape of y_p deviates from the square wave signal due to e, which primarily includes odd harmonics of the fundamental frequency of r. The amplitude spectrum of e is presented in Fig. 6(b), and the control system aims to compensate for these harmonics to improve positioning accuracy. The criteria for compensation is set to an amplitude spectrum e less than 0.3 μm, as shown in Fig. 6(b).

To address harmonic compensation, AFC is employed to generate compensation signals for the periodic error signal. The AFC dynamically updates learning coefficients at each sampling time, and the algorithm is governed by the following equations:

$$u_{ai}(k) = p_{ai}(k)\cos(\omega_{ai}Tk) + q_{ai}(k)\sin(\omega_{ai}Tk), \quad (11)$$
$$p_{ai}(k) = \sum_{m=1}^{k} \lambda_{ai}\, e(m)\cos(\omega_{ai}Tm + \theta_{ai}), \quad (12)$$
$$q_{ai}(k) = \sum_{m=1}^{k} \lambda_{ai}\, e(m)\sin(\omega_{ai}Tm + \theta_{ai}), \quad (13)$$

where u_{ai} is the compensation signal, p_{ai} and q_{ai} are learning coefficients, λ_{ai} is a step size parameter, θ_{ai} is the phase parameter, ω_{ai} is the angular frequency of u_{ai}, and k is the sample number. i denotes the $i-$th AFC. Multiple instances of AFC are employed to compensate for harmonics up to 210 Hz, as shown in Fig. 6(b). For this AFC algorithm, it is crucial to design the parameters ω_{ai}, λ_{ai}, and θ_{ai}. In particular, an adaptive algorithm can be transformed into a transfer function using convolution theory [10], [18].

$$F_{ai}(z) = \lambda_{ai}\frac{\cos(\theta_{ai}) - \cos(\omega_{ai}T + \theta_{ai})z^{-1}}{1 - 2\cos(\omega_{ai}T)z^{-1} + z^{-2}} \quad (14)$$

Researches have suggested that these parameters be designed based on the frequency response of F_{ai} [19], [20]. Specifically, ω_{ai} should match the harmonic frequency of r, λ_{ai} controls the convergence speed of the adaptive algorithm, and the value is decided by the specification with reference to the previous study. θ_{ai} determines the stability of the learning algorithm, and the value is controlled by the frequency response of the control scheme. The design strategy adopted for θ_{ai} is discussed in the following subsection.

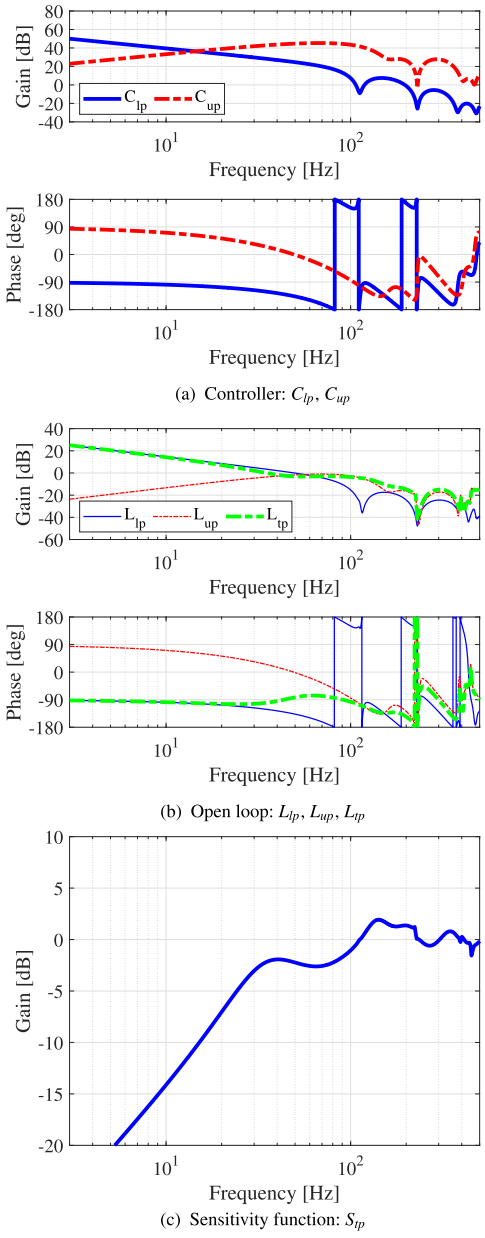

(a) Controller: C_{lp}, C_{up}

(b) Open loop: L_{lp}, L_{up}, L_{tp}

(c) Sensitivity function: S_{tp}

FIGURE 5. The characteristics of basic control system.

A. DESIGN OF θ_{AI} IN PREVIOUS CONTROL SCHEME

θ_{ai} is designed based on the previous control scheme [11], [12]. The block diagram is described as shown in Fig. 7, where $L_{lp} = P_{lp}C_{lp}$ denotes the open loop of lower piezo actuator, $L_{up} = P_{up}C_{up}$ represents the open loop of upper piezo actuator, and $L_{tp} = L_{lp} + L_{up}$ characterizes the total open loop. The control system is conceptualized as an

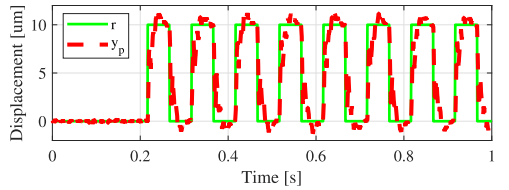

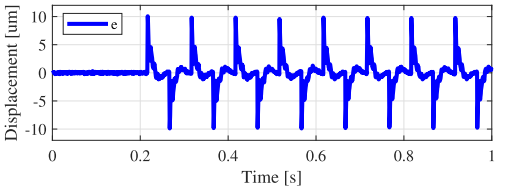

(a) The time responses: r, y_p, and e

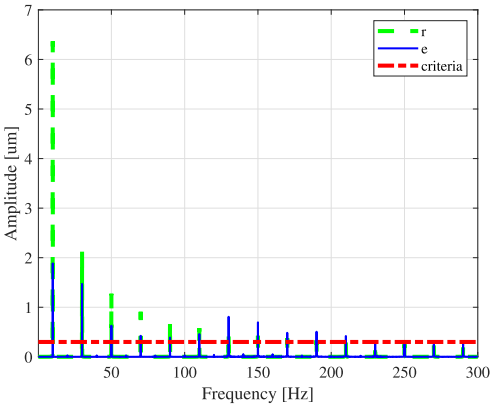

(b) The amplitude spectrum: r and e

FIGURE 6. Experimental results of the basic control system: upper figure time responses of r, y_p, and e, lower figure amplitude spectrum of r, e.

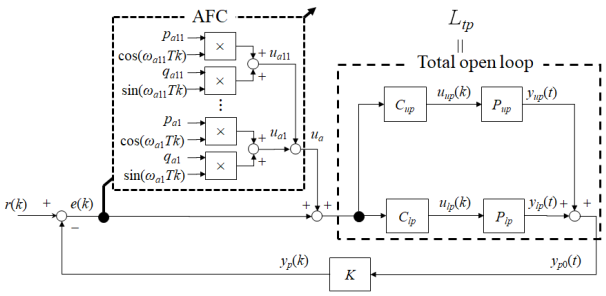

FIGURE 7. Block diagram of the DISO control system with the AFC.

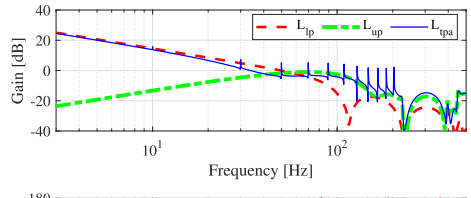

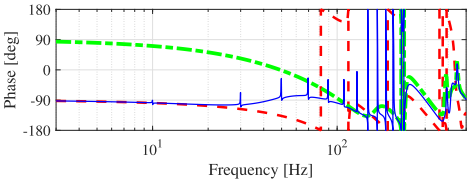

(a) Open loop: L_{lp}, L_{up}, L_{tpa}

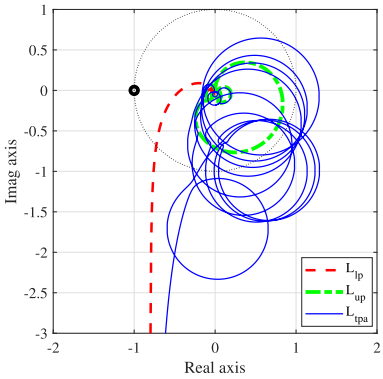

(b) Vector locus: L_{lp}, L_{up}, L_{tpa}

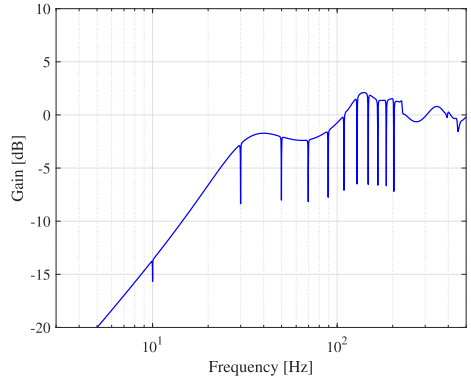

(c) Sensitivity function: S_{tpa}

FIGURE 8. The characteristics of control system with AFC based on previous control scheme.

implementation of the filter for L_{tp}. In this case, the control scheme is applied to the AFC, given that these methods are representative compensation methods for the periodic disturbance. Starting from the AFC output, u_a, to the total displacement, y_p, the control system can be treated as a SISO system. Therefore, we can apply the SISO controller design method for design of θ_{ai}, which is a major advantage of the control scheme.

Previous studies have focused on the optimal value of θ_{ai} dependent on the phase characteristics of the open loop and the control object. In this control scheme, the optimal value is described as the following equation:

$$\theta_{ai} = -\angle \frac{L_{tp}(e^{-j\omega_{ai}T})}{1 + L_{tp}(e^{-j\omega_{ai}T})} \tag{15}$$

When θ_{ai} is set as eq.(15), the vector locus of L_{tp} is far away from the unstable point $[-1, 0]$. The designed parameters are shown in Table 5. The frequency responses in the previous control schemes are shown in Fig. 8. The open loop of total open is denoted as $L_{tpa} = (1 + \sum_{i=1}^{11} F_{ai})L_{tp}$, and the sensitivity function is $S_{tpa} = \frac{1}{1+L_{tpa}}$. Sharp peaks are evident at ω_{ai} in the gain characteristic of the open loop. The Nyquist diagram indicates a circular shape in the vector locus of F_{ai}, with the circle's direction far from the unstable point, $[-1, 0]$. The control system demonstrates satisfactory gain and phase margins: 15.92 dB and 74.29 deg, respectively, with a sensitivity function exhibiting a sharp drop in gain at ω_{ai}. The maximum gain is less than 6 dB.

TABLE 5. Summary of design results F_{ai}.

i	ω_{ai} [rad/s]	θ_{ai} [deg]	λ_{ai}
1	$10\times2\pi$	-11.23	2.5×10^{-3}
2	$30\times2\pi$	-43.26	2.5×10^{-3}
3	$50\times2\pi$	-50.04	2.5×10^{-3}
4	$70\times2\pi$	-46.72	2.5×10^{-3}
5	$90\times2\pi$	-55.16	2.5×10^{-3}
6	$110\times2\pi$	-70.19	2.5×10^{-3}
7	$130\times*2\pi$	-94.56	2.5×10^{-3}
8	$150\times2\pi$	-117.16	2.5×10^{-3}
9	$170\times2\pi$	-119.38	2.5×10^{-3}
10	$190\times2\pi$	-128.45	2.5×10^{-3}
11	$210\times2\pi$	-150.40	2.5×10^{-3}

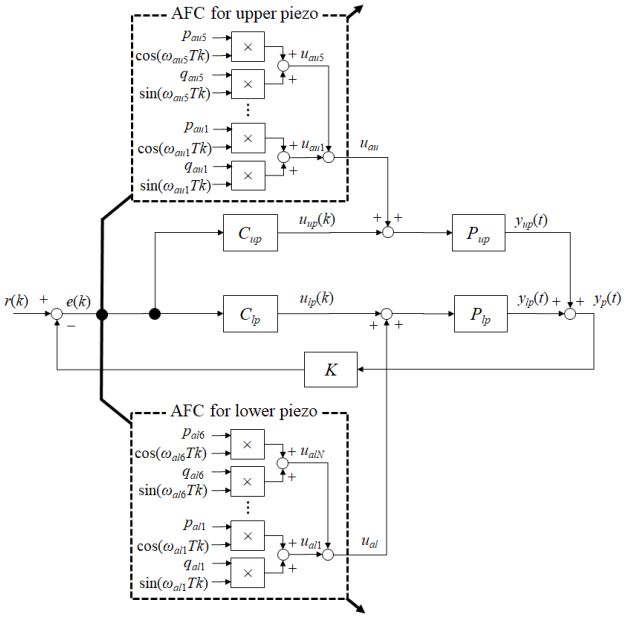

FIGURE 9. The block diagram of the DISO control system with AFC designed by the proposed method.

B. DESIGN OF θ_{AI} IN PROPOSED CONTROL SCHEME

In this study, we propose a novel control scheme for implementation of AFC in the DISO control system. The block diagram of the control system is shown in Fig. 9. The proposed control scheme employs a novel approach for implementing AFC in the DISO control system. Notably, different AFCs are used for each actuator, with the subscript al referring to the lower piezo actuator, and au indicating the upper piezo actuator. The adaptive algorithm and transfer function of AFC for each actuator are expressed as follows:

$$u_{a(l,u)i}(k) = p_{a(l,u)i}(k)\cos(\omega_{a(l,u)i}Tk) + q_{a(l,u)i}(k)\sin(\omega_{a(l,u)i}Tk) \quad (16)$$

$$p_{a(l,u)i}(k) = \sum_{m=1}^{k} \lambda_{a(l,u)i}\, e(m)\cos(\omega_{a(l,u)i}Tm + \theta_{a(l,u)i}) \quad (17)$$

$$q_{a(l,u)i}(k) = \sum_{m=1}^{k} \lambda_{a(l,u)i}\, e(m)\sin(\omega_{a(l,u)i}Tm + \theta_{a(l,u)i}) \quad (18)$$

TABLE 6. Summary of design results of F_{ali}, F_{aui}.

i	ω_{ali} [rad/s]	θ_{ali} [deg]	λ_{ali}
1	$10\times2\pi$	48.27	3.3×10^{-3}
2	$30\times2\pi$	32.71	3.3×10^{-3}
3	$50\times2\pi$	-3.80	3.3×10^{-3}
4	$70\times2\pi$	-64.82	3.3×10^{-3}
5	$90\times2\pi$	-96.23	3.3×10^{-3}
6	$210\times2\pi$	-122.47	3.3×10^{-3}
i	ω_{aui} [rad/s]	θ_{aui} [deg]	λ_{aui}
1	$110\times2\pi$	-69.90	2.4×10^{-3}
2	$130\times2\pi$	-101.63	2.4×10^{-3}
3	$150\times2\pi$	-115.36	2.4×10^{-3}
4	$170\times2\pi$	-83.48	2.4×10^{-3}
5	$190\times2\pi$	-84.61	2.4×10^{-3}

$$F_{a(l,u)i}(z) = \lambda_{a(l,u)i}\frac{\cos(\theta_{a(l,u)i}) - \cos(\omega_{a(l,u)i}T + \theta_{a(l,u)i})z^{-1}}{1 - 2\cos(\omega_{a(l,u)i}T)z^{-1} + z^{-2}} \quad (19)$$

The designed parameters are listed in Table 6 and the total number of AFCs is eleven, matching the previous control scheme. This proposed method optimizes the value of θ_{ali} and θ_{aui} for the open loop of each actuator based on the following equations:

$$\theta_{ali} = -\angle\frac{P_{dlp}(e^{-j\omega_{ali}T})}{1 + L_{lp}(e^{-j\omega_{ali}T})} \quad (20)$$

$$\theta_{aui} = -\angle\frac{P_{dup}(e^{-j\omega_{aui}T})}{1 + L_{up}(e^{-j\omega_{aui}T})} \quad (21)$$

Two key features of this design include Stoke-oriented design and robust design:

- Stoke oriented design
  The AFCs designed to compensate for lower harmonics up to $90 \times 2\pi$ are applied to the open loop of the lower piezo actuator. This choice is driven by the relatively large amplitude of lower harmonics, as evident in Fig. 6. The necessity for a large stroke to track r and compensate for e in the lower harmonics makes it suitable for the lower piezo actuator, which has a larger stroke. Conversely, the upper piezo actuator is engaged in handling higher harmonics with relatively smaller amplitudes. This design approach aligns with the concept of coarse-fine motion control.
- Robust design
  Referring to Fig. 2, the lower piezo actuator exhibits a mechanical resonance at 112 Hz, while the upper piezo actuator's resonance occurs at 225 Hz. In the presence of mechanical characteristic variations leading to changes in resonance frequency, the optimal values of θ_{ali} and θ_{aui} calculated by Eqs.(20) and (21) are also subject to change. To mitigate the impact of mechanical variations, the proposed design implements AFCs around 110 Hz for the upper piezo actuator and around 220 Hz for the lower piezo actuator.

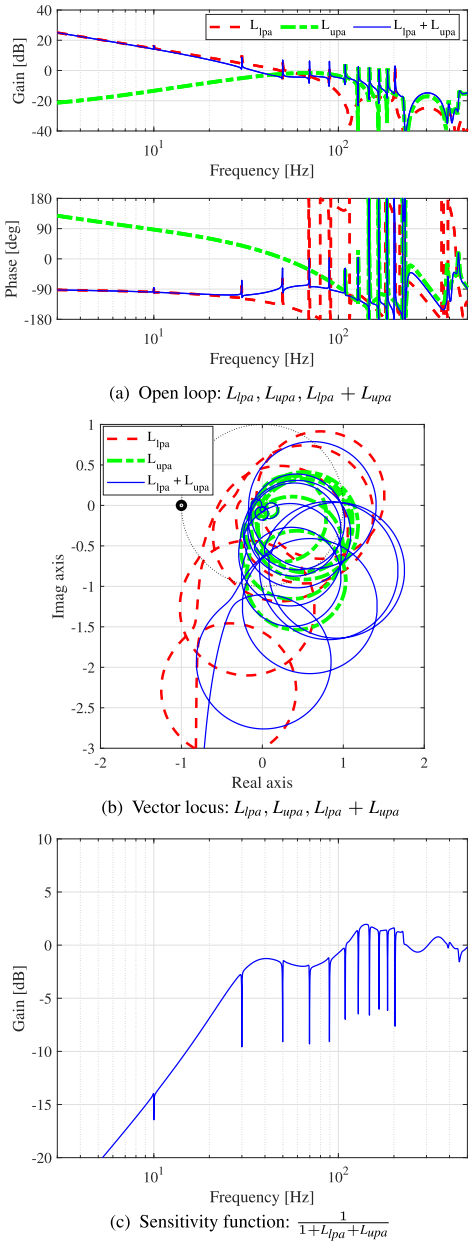

(a) Open loop: L_{lpa}, L_{upa}, $L_{lpa} + L_{upa}$

(b) Vector locus: L_{lpa}, L_{upa}, $L_{lpa} + L_{upa}$

(c) Sensitivity function: $\frac{1}{1+L_{lpa}+L_{upa}}$

FIGURE 10. The characteristics of control system with AFC based on the proposed control scheme.

The frequency responses of the proposed control scheme are illustrated in Fig. 10. In this representation, the open loop of the lower actuator is denoted as $L_{lpa} = (1 + \sum_{i=1}^{6} F_{ali})L_{lp}$, the open loop of the upper actuator is expressed as $L_{upa} = (1 + \sum_{i=1}^{5} F_{aui})L_{up}$, and the total actuator's open loop is characterized by $L_{lpa} + L_{upa}$. Additionally, the sensitivity function is captured by $\frac{1}{1+L_{lpa}+L_{upa}}$. While the frequency response of the total actuator's open loop and sensitivity function align closely with those of the previous control scheme, variations arise in the frequency response of each actuator's open loop. These discrepancies stem from the distinct design concepts employed for the AFC in each actuator.

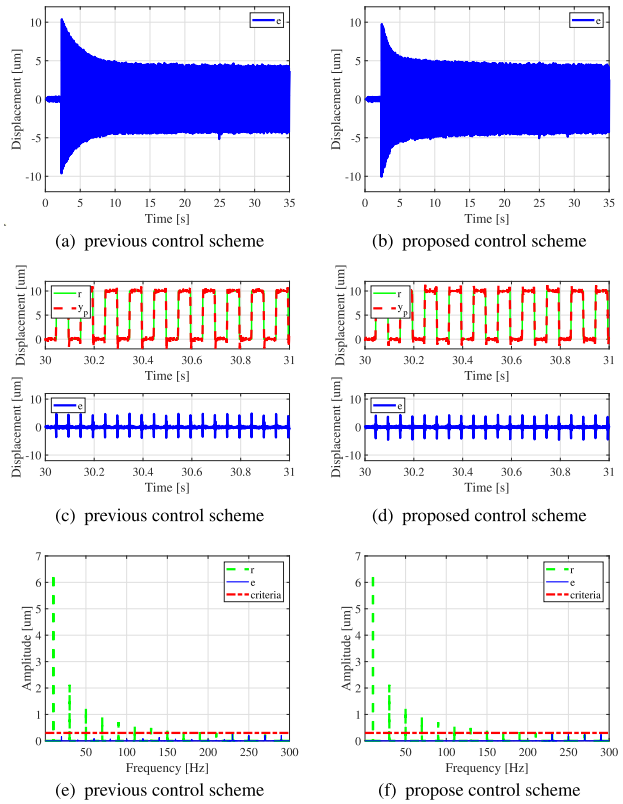

(a) previous control scheme (b) proposed control scheme

(c) previous control scheme (d) proposed control scheme

(e) previous control scheme (f) propose control scheme

FIGURE 11. Experimental Results of the Tracking Control: The upper figures provide an overview of the time responses of *e*, the middle figures display time responses of *r* and y_p with a focus on the interval between 30 s and 31 s, and the lower figures present the amplitude spectrum of *r* and *e*.

TABLE 7. Summary of standard deviation of the displacement signal.

Control scheme	σ of y_{lp}	σ of y_{up}	σ of y_{tp}
Previous	9.09	5.47	4.91
Proposed	7.80	2.98	4.93
Differential rate	-14%	-45%	0%

V. EXPERIMENTAL VERIFICATION

In this section, we conducted an experimental comparison study between the previous control scheme outlined in Section IV-A and the proposed control scheme detailed in Section IV-B, focusing on the repetitive motion tracking of a 10 Hz square wave signal denoted as r.

First, we address the fundamental performance of both control schemes. Figs. 11(a) and (b) depict the time responses of e during the convergence of the adaptive algorithm of AFCs, which stabilizes in approximately 30 seconds. Subsequently, both control schemes exhibit enhanced tracking performance for r, as evident in Figs. 11(c) and (d). Moreover, they effectively compensate for the harmonics of e up to 210 Hz, meeting the criteria for the amplitude spectrum, as illustrated in Figs. 11(e) and (f).

Secondly, we verified the stroke-oriented design within the proposed control scheme. The time responses of the displacement for each actuator are presented in Fig. 12. While

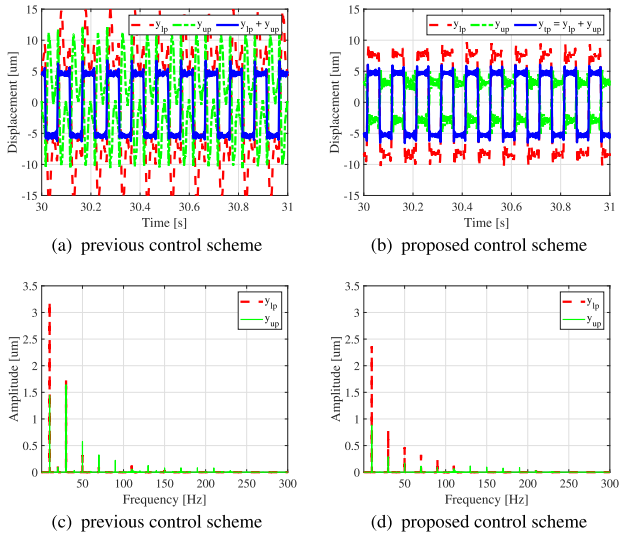

FIGURE 12. Experimental results of the actuator displacement are depicted in the upper figures, showcasing the time responses of y_{lp}, y_{up}, and the total displacement $y_{tp} = y_{lp} + y_{up}$. In the lower figures, the amplitude spectrum of y_{lp} and y_{up} is illustrated.

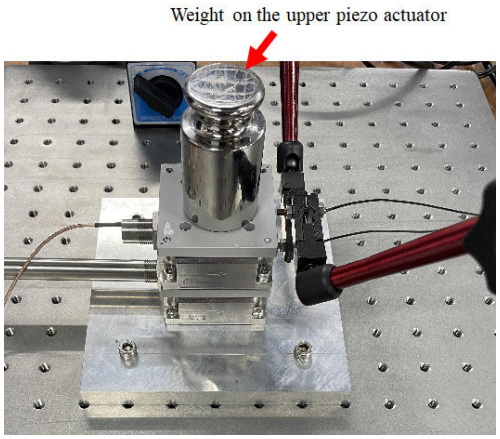

FIGURE 13. Experimental system of the DISO system with weight.

the total displacement $y_{tp} = y_{lp} + y_{up}$ remains almost identical in both control schemes, a noticeable disparity emerges in the displacement of each actuator, namely y_{lp} and y_{up}, between the previous and proposed control schemes. In the previous control scheme, the AFC is applied to the open loop of the total actuator L_{tp}; consequently, all AFCs function for both actuators. In contrast, the proposed control scheme employs separate AFCs for each open loop, aligning with the concept of a coarse-fine motion system. This approach prevents unnecessary movement for the actuators, particularly minimizing the motion of the upper piezo actuator in the low-frequency range. The summary of standard deviation σ is detailed in Table 7. Although the value of σ for y_{tp} is nearly the same in both control schemes, the σ values for y_{lp} or y_{up} are reduced when utilizing the proposed control scheme.

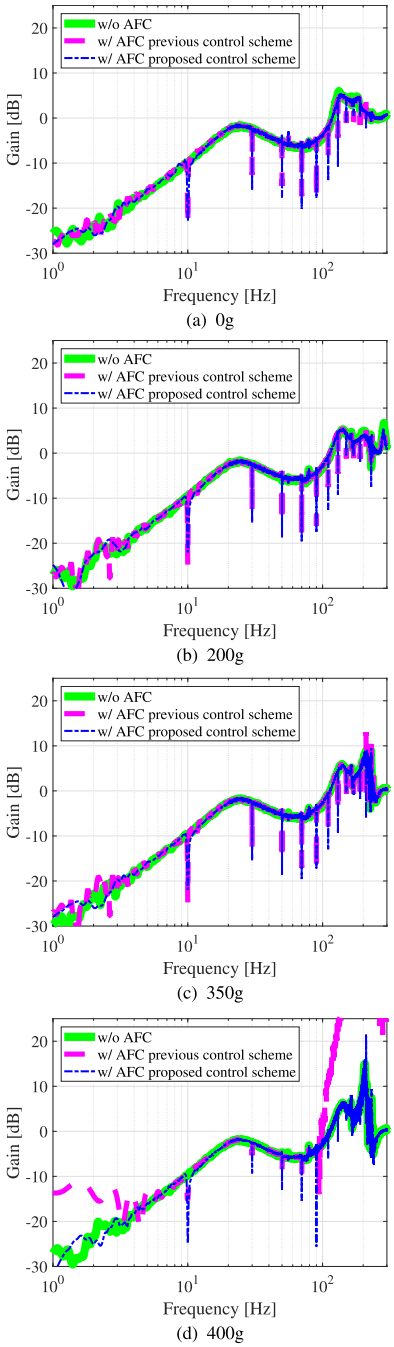

FIGURE 14. Experimental results of the gain of sensitivity function of without AFC, with AFC previous control scheme, with AFC proposed control scheme: 0g, 200g, 350g, and 400g from the top.

TABLE 8. Maximum gain of the sensitivity function.

Control scheme	0g	200g	350g	400g
w/o AFC	5.40 dB	5.68 dB	9.01 dB	15.02 dB
Previous	5.45 dB	5.58 dB	13.06 dB	unstable
Proposed	5.42 dB	5.54 dB	9.36 dB	21.55dB

Thirdly, we assessed the robustness of both control schemes. To conduct this evaluation, additional weight was applied to the upper piezo actuator, as depicted in Fig. 13.

The gain of the sensitivity function was calculated through sine sweep tests carried out with weights of 0, 200, 350, and 400g. The sine sweep signal was utilized as the input signal denoted by r, and the gain was computed using the following equation.

$$20\log_{10}\left|\frac{\mathcal{F}[e(k)]}{\mathcal{F}[r(k)]}\right| \tag{22}$$

where $\mathcal{F}[e(k)]$ and $\mathcal{F}[r(k)]$ denote the Fourier transforms of e and r, respectively. The results of the calculations are depicted in Fig. 14, where the nominal case (without weight: 0g) is also included. Furthermore, a case without AFC, as discussed in Section III, is presented for comparison purposes. Figs. 14(a), (b), (c) and (d) indicate the gain of the sensitivity function calculated from the experimental data with weights of 0, 200, 350, and 400g, respectively. In all control schemes, the gain of the sensitivity function experiences an increase around 220 Hz with the addition of weight. This phenomenon is attributed to the reduction in the resonance frequency of the upper piezo actuator, originally at 225 Hz, as the weight is augmented. In the previous control scheme, the optimal value of θ_{ai} deviates from the designed value in the nominal case. Specifically, the value of θ_{a11} for the 11th AFC, which compensates for the 210 Hz harmonics, is notably affected by mechanical variations. Consequently, the control system fails to maintain stable operation in the presence of the attached 400g weight. Conversely, the proposed control scheme allows for the independent implementation of AFCs for each actuator. In this setup, the AFC compensating for the 210 Hz harmonics is specifically applied to the lower piezo actuator, which lacks mechanical resonance. Consequently, the optimal value of θ_{al6} is less influenced by mechanical variations. The maximum gain of the sensitivity function is shown in Table 8. That of the values of proposed control scheme remains nearly identical to that of the control scheme without AFC up to 350g. In addition, the proposed control scheme can sustain stable operation even with 400g weight attached.

In summary, AFCs contribute to enhancing the tracking performance for repetitive motion in both control schemes. Importantly, the proposed control scheme exhibits improved robustness with reduced actuator movements compared to the previous control scheme.

VI. CONCLUSION

This study introduces a novel control scheme designed to achieve precise repetitive motion within the DISO system. The proposed control system incorporates AFC to effectively compensate for position error signals induced by repetitive motion, thereby enhancing tracking performance. The outlined control scheme offers several notable advantages.

Firstly, the integration of AFC into the control system successfully diminishes position error signals during repetitive motion, leading to a substantial improvement in tracking accuracy. Secondly, the control scheme considers the stroke limitations of each actuator, allowing for the optimization of control performance suitable for coarse-fine motion control. This aspect is particularly advantageous in applications where such considerations are crucial. Thirdly, the proposed control scheme demonstrates robustness against uncertainties inherent in the system, a critical feature for real-world applications where mechanical variations in system parameters are commonplace.

Experimental results underscore the effectiveness of the proposed control scheme. Notably, it showcases improvements in tracking performance, a reduction in the displacement of each actuator when compared to the previous control scheme, and the ability to maintain stable operation despite the influence of mechanical variations. The proposed control scheme, thus, emerges as a valuable enhancement for control performance in DISO systems, especially in applications demanding precise repetitive motion, such as those found in manufacturing processes.

DECLARATION OF CONFLICTING INTERESTS

The authors declare no conflicts of interest in preparing this article.

REFERENCES

[1] J. Doyle, B. Francis, and A. Tannenbaum, *Feedback Control Theory*. New York, NY, USA: Dover, 2009.

[2] U. Boettcher, B. Raeymaekers, R. A. de Callafon, and F. E. Talke, "Dynamic modeling and control of a piezo-electric dual-stage tape servo actuator," *IEEE Trans. Magn.*, vol. 45, no. 7, pp. 3017–3024, Jul. 2009.

[3] S. Yabui, T. Atsumi, and T. Inoue, "Coupling controller design for MISO system of head positioning control systems in HDDs," *IEEE Trans. Magn.*, vol. 56, no. 5, pp. 1–9, May 2020.

[4] M. Stalder, Y. Michellod, P. Mullhaupt, and D. Gillet, "Dedicated controller design for a dual-stage opto-mechatronic system," in *Proc. IEEE/ASME Int. Conf. Adv. Intell. Mechatronics*, Jul. 2008, pp. 457–464.

[5] Z. Wu, X. Chen, W. Hua, and J. Wang, "Design of coarse-fine control system for wafer stage of lithography using PQ method," in *Proc. 3rd Int. Symp. Syst. Control Aeronaut. Astronaut.*, Harbin, China, Jun. 2010, pp. 660–664.

[6] H. Chun, J. Han, L. Wright, A. Elwany, H. Villarraga-Gómez, and C. Lee, "Pressure-fed mechanism to compensate for motions and dynamic characteristics of compliant nanopositioning stages," *Precis. Eng.*, vol. 63, pp. 33–40, May 2020.

[7] B. B. Muhammad, M. Bashir, M. F. Hamza, M. Abdulhadi, M. A. Shehu, S. K. Debnath, and S. Bagchi, "A feedback controller for milling chatter vibration control using a new response matrix," *J. Vibrat. Control*, vol. 28, nos. 9–10, pp. 998–1010, May 2022.

[8] M. Bodson, A. Sacks, and P. K. Khosla, "Harmonic generation in adaptive feedforward cancellation schemes," *IEEE Trans. Autom. Control*, vol. 39, no. 9, pp. 1939–1944, Sep. 1992.

[9] A. Sacks, M. Bodson, and P. Khosla, "Experimental results of adaptive periodic disturbance cancellation in a high performance magnetic disk drive," in *Proc. Amer. Control Conf.*, Jun. 1993, pp. 690–6860.

[10] W. Messner and M. Bodson, "Design of adaptive feedforward controllers using internal model equivalence," in *Proc. Amer. Control Conf. (ACC)*, Baltimore, MD, USA, Jun. 1994, pp. 1619–1623.

[11] X. Chen and M. Tomizuka, "Discrete-time reduced-complexity Youla parameterization for dual-input single-output systems," *IEEE Trans. Control Syst. Technol.*, vol. 24, no. 1, pp. 302–309, Jan. 2016.

[12] A. Gams, B. Nemec, A. J. Ijspeert, and A. Ude, "Coupling movement primitives: Interaction with the environment and bimanual tasks," *IEEE Trans. Robot.*, vol. 30, no. 4, pp. 816–830, Aug. 2014.

[13] H. K. Shirvani, Y. Hosseinkhani, and K. Erkorkmaz, "Suppression of harmonic positioning errors in ball-screw drives using adaptive feedforward cancellation," *Precis. Eng.*, vol. 68, pp. 235–255, Mar. 2021.

[14] S. J. Schroeck and W. C. Messner, "On controller design for linear time-invariant dual-input single-output systems," in *Proc. Amer. Control Conf.*, San Diego, CA, USA, Jun. 1999, pp. 4122–4126.
[15] N. A. Weir and A. G. Alleyne, "Controller design for two-input single-output systems exploiting plant/controller alignment," in *Proc. Adv. Control Design Methods; Adv. Nonlinear Control; Adv. Robot.; Assistive Rehabil. Robotics; Automot. Dyn. Emerg. Powertrain Technol.; Automot. Systems; Bio Eng. Appl.; Bio-Mechatronics Phys. Hum. Robot Interact.; Biomed. Neural Syst.; Biomed. Neural Syst. Modeling, Diag., Healthcare*, Atlanta, Georgia, Sep. 2018, Art. no. V001T01A012.
[16] J. Xia, Z. Guo, and Z. Li, "Optimal online resonance suppression in a drive system based on a multifrequency fast search algorithm," *IEEE Access*, vol. 9, pp. 55373–55387, 2021.
[17] S. Yabui and T. Atsumi, "High-bandwidth controller design for dual-stage actuator system in hard disk drives," *J. Vibrat. Control*, vol. 29, nos. 5–6, pp. 1268–1279, Mar. 2023.
[18] S. Yabui, A. Okuyama, M. Kobayashi, and T. Atsumi, "Optimization of adaptive feedforward repeatable run-out cancellation for positioning control system of hard disk drives," *Microsyst. Technol.*, vol. 18, nos. 9–10, pp. 1703–1709, Sep. 2012.
[19] S. Yabui, A. Okuyama, T. Atsumi, and M. Odai, "Development of optimized adaptive feed-forward cancellation with damping function for head positioning system in hard disk drives," *J. Adv. Mech. Design, Syst., Manuf.*, vol. 7, no. 1, pp. 39–51, 2013.
[20] S. Yabui and T. Inoue, "Development of optimal controller design method to compensate for vibrations caused by unbalanced force in rotor system based on Nyquist diagram," *J. Vibrat. Control*, vol. 25, no. 4, pp. 793–805, Feb. 2019.

SHOTA YABUI (Member, IEEE) received the B.S. and M.S. degrees in electrical engineering from Mie University, Tsu, Japan, in 2007 and 2009, respectively, and the Ph.D. degree in mechanical engineering from Hokkaido University, Sapporo, Japan, in 2014. From 2009 to 2015, he was with Hitachi Ltd., and HGST Japan, to develop control technologies for hard disk drives. In 2016, he was with Mitsubishi Space Software Company Ltd., to analyze flight dynamics for Mitsubishi regional jet. Since 2021, he has been an Associate Professor with the Department of Mechanical Systems Engineering, Faculty of Science and Engineering, Tokyo City University. His research interests include adaptive feed-forward control technologies, integrated design methods of control and mechanics, and analysis of rotor dynamics. He is a member of JSME, IEEJ, and ASME. He was awarded the MEXT Young Scientists' Prize, in 2023.

HARUKI MURAKAMI (Member, IEEE) received the B.S. degree in mechanical systems engineering from Tokyo City University, Tokyo, Japan, in 2022, where he is currently pursuing the M.S. degree in mechanical engineering.

TAKENORI ATSUMI (Member, IEEE) received the B.S., M.S., and Ph.D. degrees in mechanical engineering from Chiba University, Chiba, Japan, in 1997, 1999, and 2006, respectively. He started his career with the Mechanical Engineering Research Laboratory, Hitachi Ltd., Japan, in 1999. From 2009 to 2010, he was a Visiting Fellow with the Data Storage Systems Center (DSSC), Carnegie Mellon University. He was with Hitachi Ltd., and HGST Japan, from 1999 to 2015, where he developed control technologies for hard disk drives. He joined the Chiba Institute of Technology, in 2015. He is currently with the Department of Mechanical Engineering, Chiba Institute of Technology, Narashino, Japan. He is a member of the Society of Instrument and Control Engineers of Japan (SICE), Japan Society of Mechanical Engineers (JSME), and the Institute of Electrical Engineers of Japan (IEEJ).

YUSUKE UCHIYAMA received the B.S. and M.S. degrees in mechanical engineering and the Ph.D. degree in mathematical engineering from the University of Tsukuba, Tsukuba, Japan, in 2007, 2009, and 2014, respectively. From 2009 to 2012, he was with Hitachi Ltd., Japan, to develop numerical analysis and optimization technologies for turbomachinery. In 2012, he was with the University of Tsukuba to analyze complex time-series data and to develop stochastic models for non-ergodic systems. Since 2018, he has been the Research Director of MAZIN Inc., to engage in studying and developing applications of machine learning for the manufacturing industry. His research interests include applications of stochastic processes, Bayesian modeling, and nonlinear dynamics. He is a member of JPS, JSAI, JSME, and JAFEE. He was awarded the JSAI Best Research Prize, in 2020.